Investigating the role of background and observation error correlations in improving a model forecast of forest carbon balance using 4D-Var.

Ewan Pinnington, E. Casella, S. L. Dance, A. S. Lawless, J. I. L. Morison,
N. K. Nichols, T. L. Quaife, M. Wilkinson add affiliations

December 15, 2015

Abstract

Efforts to implement variational data assimilation routines with functional ecology models and land surface models have been limited, with sequential and Markov chain Monte Carlo data assimilation methods being prevalent. When data assimilation has been used with models of carbon balance, background "prior" errors and observation errors have largely been treated as independent and uncorrelated. Correlations between background errors have long been known to be a key aspect of data assimilation in numerical weather prediction. More recently, it has been shown that accounting for correlated observation errors in the assimilation algorithm can considerably improve data assimilation results and forecasts. In this paper we implement a Four-Dimensional Variational data assimilation (4D-Var) scheme with a simple model of forest carbon balance, for joint parameter and state estimation and assimilate daily observations of Net Ecosystem CO_2 Exchange (NEE) taken at the Alice Holt forest CO_2 flux site in Hampshire, UK. We then investigate the effect of specifying correlations between parameter and state variables in background error statistics and the effect of specifying correlations in time between observation error statistics. The idea of including these correlations in time is new and has not been previously explored in carbon balance model data assimilation. In data assimilation, background and observation error statistics are often described by the background error covariance matrix and the observation error covariance matrix. We outline novel methods for creating correlated versions of these matrices, using a set of previously postulated dynamical constraints to include correlations in the background error statistics and a Gaussian correlation function to include time correlations in the observation error statistics. The methods used in this paper will allow the inclusion of time correlations between many different observation types in the assimilation algorithm, meaning that previously neglected information can be accounted for. In our experiments we compared the results using our new correlated background and observation error covariance matrices and those using diagonal covariance matrices. We found that using the new correlated matrices reduced the root mean square error in the 14 year forecast of daily NEE by 44% decreasing from $4.22\text{gCm}^{-2}\text{day}^{-1}$ to $2.38\text{gCm}^{-2}\text{day}^{-1}$.

1 Introduction

The land surface and oceans are responsible for removing around half of all human emitted carbon-dioxide from the atmosphere and therefore mediate the effect of anthropogenic induced climate change. Terrestrial ecosystem carbon uptake is the least understood process in the global carbon cycle [Ciais et al., 2014]. It is therefore vital that we improve understanding of the carbon uptake of terrestrial ecosystems and their response to climate change in order to better constrain predictions of future carbon budgets. Observations of the Net Ecosystem Exchange (NEE) of CO_2 between terrestrial ecosystems and the atmosphere are now routinely made at flux tower sites world-wide, at sub-hourly resolution and covering

multiple years [Baldocchi, 2008], providing a valuable resource for carbon balance model validation and data assimilation.

Data assimilation is the process of combining a mathematical model with observations in order to improve the estimate of the state of a system. Data assimilation has successfully been used in many applications to significantly improve model state and forecasts. Perhaps the most important application has been in numerical weather prediction where data assimilation has contributed to the forecast accuracy being increased at longer lead times, with the four day forecast in 2014 having the same level of accuracy as the one day forecast in 1979 [Bauer et al., 2015]. This increase in forecast skill is obviously not solely due to data assimilation but also increased quality and resolution of observations along with improvements in model structure, however the introduction and evolution of data assimilation has played a large part [Dee et al., 2011]. The current method implemented at many leading operational numerical weather prediction centres is known as Four-Dimensional Variational data assimilation (4D-Var) [Bonavita et al., 2015, Clayton et al., 2013], which has been shown to be a significant improvement over its predecessor three-dimensional variational assimilation [Lorenc and Rawlins, 2005]. Variational assimilation techniques minimise a cost function to find the optimal state of a system given all available knowledge of errors in the model and observations. The minimisation routine typically requires the derivative of the model which can sometimes prove difficult to calculate. Using techniques such as automatic-differentiation [Renaud, 1997] can reduce the time taken to implement the derivative of a model. In numerical weather prediction data assimilation has been predominately used for state estimation whilst keeping parameters fixed. Variational data assimilation can be used for joint parameter and state estimation by augmenting the state vector with the parameters [Navon, 1998]. By including the parameters in the state vector we must also specify error statistics and error correlations for them. Smith et al. [2009] show that the prescription of these error statistics and their correlations can have a significant impact on parameter-state estimates obtained from the assimilation.

Many different observations relevant to the carbon balance of forests have now been combined with functional ecology models, using data assimilation, in order to improve our knowledge ecological systems [Fox et al., 2009, Niu et al., 2014, Quaife et al., 2008, Richardson et al., 2010, Zobitz et al., 2014, 2011]. Two such models that have been used extensively with data assimilation are the Data Assimilation Linked Ecosystem Carbon (DALEC) model [Williams et al., 2005] and the Simplified Photosynthesis and Evapo-Transpiration (SIPNET) model [Braswell et al., 2005]. Nearly all data assimilation routines built with these models have used sequential and Monte Carlo Markov chain (MCMC) data assimilation methods with the exception of a variational routine being implemented for DALEC by Delahaies et al. [2013]. There have been examples of global land surface models being implemented with variational methods such as the ORganizing Carbon and Hydrology In Dynamic EcosystEms model (ORCHIDEE) [Krinner et al., 2005] and the Biosphere Energy Transfer HYdrology scheme (BETHY) in a Carbon Cycle Data Assimilation System (CCDAS) [Kaminski et al., 2013]. These examples have mainly been used to assimilate data from satellite and atmospheric CO_2 observations with only a few cases where site level data has also been assimilated [Bacour et al., 2015, Verbeeck et al., 2011].

Background errors (describing our knowledge of error in prior model estimates before data assimilation) and observation errors have largely been treated as uncorrelated and independent in ecosystem model data assimilation schemes. In 3D and 4DVar schemes background and observation errors are represented by the error covariance matrices $\mathbf{B}$ and $\mathbf{R}$ respectively. The off-diagonal elements of these matrices indicate the correlations between the parameter and state variables for $\mathbf{B}$ and the correlations between observation errors for $\mathbf{R}$. In the assimilation, the off-diagonal terms in the $\mathbf{B}$ matrix act to spread information between the state and augmented parameter variables [Kalnay, 2003]. This means that assimilating observations of one state variable can act to update different state and parameter variables in the assimilation when correlations are included in $\mathbf{B}$. In 4D-Var the $\mathbf{B}$ matrix is propagated implicitly by the forecast model, so that even a propagated diagonal $\mathbf{B}$ matrix can develop correlations throughout an assimilation window. These correlations will only be in the propagated $\mathbf{B}$ matrix, with the $\mathbf{B}$ matrix valid at the initial time remaining unchanged. Including correlations in $\mathbf{B}$ has been shown to significantly

improve data assimilation results in numerical weather prediction [Bannister, 2008].

Including correlations between observation errors has only started to be explored recently in numerical weather prediction, with $\mathbf{R}$ still often treated as diagonal [Stewart et al., 2013]. Including some correlation structure in $\mathbf{R}$ has been shown to improve forecast accuracy [Weston et al., 2014]. Currently the correlations included in $\mathbf{R}$ have been mainly between observations made at the the same time rather than correlations between observations throughout time. When assimilating observations, data streams with many more observations can have a greater impact on the assimilation than those with fewer observations. In Richardson et al. [2010] this problem is discussed when assimilating large numbers of NEE observations along with smaller numbers of leaf area index and soil respiration observations. To address this problem Richardson et al. uses a cost function that calculates the product of the departures from the observations rather than a cost function which sums these departures, giving a relative rather than absolute measure of the goodness-of-fit to the observations. This problem is also encountered in Bacour et al. [2015] when assimilating daily eddy covariance data with weekly observations of the FrAction of Photosynthetically Active Radiation (FAPAR). In Bacour et al. [2015] the error in observations of FAPAR is divided by two in order to give these less frequent observations more weight in the assimilation algorithm. Specifying serial time correlations between observations represents another way of addressing this problem, whilst also adding valuable information to the data assimilation routine. Including serial correlations between observations of the same quantity decreases the impact of these observations [Järvinen et al., 1999] therefore increasing the impact of less frequent observations.

In this paper we implement the new version of DALEC (DALEC2 [Bloom and Williams, 2015]) in a 4D-Var data assimilation scheme for joint state and parameter estimation, assimilating daily NEE observations from the Alice Holt flux site in Hampshire, UK [Wilkinson et al., 2012]. This assimilation scheme is then subjected to rigorous testing to ensure correctness. A new method is outlined for including parameter and state correlations in the background error covariance matrix. Currently parameter and state error statistics are largely treated as independent and uncorrelated when data assimilation has been used with models of carbon balance. We also introduce a novel method for including serial time correlations in the observation error covariance matrix. The idea of including time correlations between observation error statistics is new and has not been previously explored in carbon balance model data assimilation. These correlated matrices are then used in a series of experiments in order to examine the effect that including correlations in the assimilation scheme has on the results. We show that specifying parameter and state correlations in the prior knowledge and serial correlations between observation errors can significantly improve the fit of the predicted carbon balance to observations with the root mean square error in the 14 year forecast of daily NEE decreasing by 44% from $4.22\mathrm{gCm^{-2}day^{-1}}$ to $2.38\mathrm{gCm^{-2}day^{-1}}$.

2 Model and Data Assimilation Methods

2.1 Alice Holt research forest

Alice Holt Forest is a research forest area managed by the UK Forestry Commission located in Hampshire, SE England. Forest Research has been operating a CO_2 flux measurement tower in a portion of the forest, the Straits Inclosure, since 1998 so it is one of the longer forest site CO_2 flux records, globally. The Straits Inclosure is a 90ha area of managed deciduous broadleaved plantation woodland, presently approximately 80 years old, on a surface water gley soil. The majority of the canopy trees are oak (Quercus robur), with an understory of hazel (Corylus avellana) and hawthorn (Crataegus monogyna); but there is a small area of conifers (Pinus nigra) within the tower measurement footprint area in some weather conditions. Further details of the Straits Inclosure site and the measurement procedures are given in Wilkinson et al. [2012], together with analysis of stand-scale 30 minute average net CO_2 fluxes (NEE) measured by standard eddy covariance methods from 1998-2011. The data used here span from January 1999 to December 2013, and consist of the NEE fluxes and meteorological driving data of temperatures, irradiance and atmospheric CO_2 concentration. The original NEE data were subjected to normal quality control procedures, including

u^* filtering to remove unreliable data when there were low turbulence night time conditions, as described in Wilkinson et al. [2012], but were not gap-filled. To compute daily NEE observations we take the sum over the 48 measurements made each day. We only select days where there is no missing data and over 90% of CO_2 flux observations have a quality control flag associated with the best observations and no observations associated with the worst from the EddyPro flux processing software [LI-COR, Inc., 2015].

2.2 The DALEC2 model

The DALEC2 model is a simple process-based model describing the carbon balance of a forest ecosystem [Bloom and Williams, 2015] and is the new version of the original DALEC [Williams et al., 2005]. The model is constructed of six carbon pools (labile (C_{lab}), foliage (C_f), fine roots (C_r), woody stems and coarse roots (C_w), fresh leaf and fine root litter (C_l) and soil organic matter and coarse woody debris (C_s)) linked via fluxes. The aggregated canopy model (ACM) [Williams et al., 1997] is used to calculate daily gross primary production (GPP) of the forest, taking meteorological driving data and the modelled leaf area index (a function of C_f) as arguments. Figure 1 shows a schematic of how the carbon pools are linked in DALEC2.
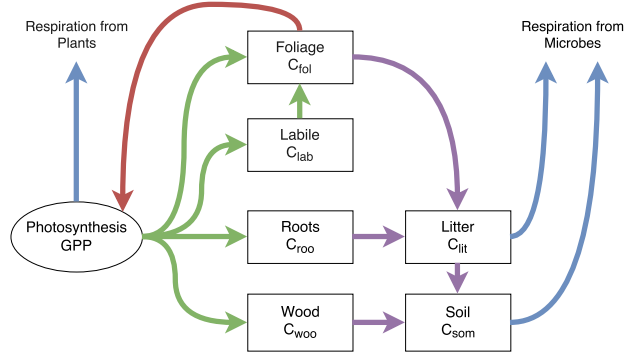

Figure 1: Representation of the fluxes in the DALEC2 carbon balance model. Green arrows represent C allocation, purple arrows represent litter fall and decomposition fluxes, blue arrows represent respiration fluxes and the red arrow represents the influence of leaf area index in the GPP function.

The model equations for the carbon pools at day $i + 1$ are as follows:

$$GPP^i = ACM(C_{fol}^{i-1}, c_{lma}, c_{eff}, \Psi) \tag{1}$$

$$C_{lab}^i = (1 - \Phi_{on})C_{lab}^{i-1} + (1 - f_{auto})(1 - f_{fol})f_{lab}GPP^i, \tag{2}$$

$$C_{fol}^i = (1 - \Phi_{off})C_{fol}^{i-1} + \Phi_{on}C_{lab}^{i-1} + (1 - f_{auto})f_{fol}GPP^i, \tag{3}$$

$$C_{roo}^i = (1 - \theta_{roo})C_{roo}^{i-1} + (1 - f_{auto})(1 - f_{fol})(1 - f_{lab})f_{roo}GPP^i, \tag{4}$$

$$C_{woo}^i = (1 - \theta_{woo})C_{woo}^{i-1} + (1 - f_{auto})(1 - f_{fol})(1 - f_{lab})(1 - f_{roo})GPP^i, \tag{5}$$

$$C_{lit}^i = (1 - (\theta_{lit} + \theta_{min})e^{\Theta T^{i-1}})C_{lit}^{i-1} + \theta_{roo}C_{roo}^{i-1} + \Phi_{off}C_{fol}^{i-1}, \tag{6}$$

$$C_{som}^i = (1 - \theta_{som}e^{\Theta T^{i-1}})C_{som}^{i-1} + \theta_{woo}C_{woo}^{i-1} + \theta_{min}e^{\Theta T^{i-1}}C_{lit}^{i-1}, \tag{7}$$

where T^{i-1} is the daily mean temperature, Ψ represents the meteorological driving data used in the GPP function and Φ_{on}/Φ_{off} are functions controlling leaf-on and leaf-off. The model parameters used in equations (1) to (7) are included in the appendix in table 3. DALEC2 differs from the original DALEC in that it can be parameterised for both deciduous and evergreen sites with Φ_{on} and Φ_{off} being able to reproduce the phenology of either type of site. The full details of this version of DALEC can be found in Bloom and Williams [2015].

2.3   4D-Var

We consider the discrete nonlinear dynamical system given by

$$\mathbf{z}_i = \mathbf{f}_{i-1 \to i}(\mathbf{z}_{i-1}, \mathbf{p}_{i-1}), \tag{8}$$

where $\mathbf{z}_i \in \mathbb{R}^n$ is the state vector at time t_i, $\mathbf{f}_{i-1 \to i}$ is the nonlinear model operator propagating the state at time t_{i-1} to time t_i for $i = 1, 2, \ldots, N$ and $\mathbf{p}_{i-1} \in \mathbb{R}^q$ is a vector of q model parameters at time t_{i-1}. For DALEC2 the state vector $\mathbf{z}_i = (C_{lab}^i, C_{for}^i, C_{roo}^i, C_{woo}^i, C_{lit}^i, C_{som}^i)^T$. The model parameters are not updated by the nonlinear model operator, therefore the evolution of the parameters is given by,

$$\mathbf{p}_i = \mathbf{p}_{i-1}, \tag{9}$$

for $i = 1, 2, \ldots, N$. We define the new vector $\mathbf{x}$ by joining the parameter vector $\mathbf{p}$ with the model state vector $\mathbf{z}$, giving us the augmented state vector

$$\mathbf{x} = \begin{pmatrix} \mathbf{p} \\ \mathbf{z} \end{pmatrix} \in \mathbb{R}^{q+n}. \tag{10}$$

We define the augmented system model by

$$\mathbf{x}_i = \mathbf{m}_{i-1 \to i}(\mathbf{x}_{i-1}), \tag{11}$$

where

$$\mathbf{m}_{i-1 \to i}(\mathbf{x}_{i-1}) = \begin{pmatrix} \mathbf{p}_{i-1} \\ \mathbf{f}_{i-1 \to i}(\mathbf{z}_{i-1}, \mathbf{p}_{i-1}) \end{pmatrix} = \begin{pmatrix} \mathbf{p}_i \\ \mathbf{z}_i \end{pmatrix} \in \mathbb{R}^{q+n}. \tag{12}$$

The available observations at time t_i are represented by the vector $\mathbf{y}_i \in \mathbb{R}^{r_i}$ which are related to the augmented state vector through the equation

$$\mathbf{y}_i = \mathbf{h}_i(\mathbf{x}_i) + \epsilon_i, \tag{13}$$

where $\mathbf{h}_i : \mathbb{R}^{q+n} \to \mathbb{R}^{r_i}$ is the observation operator mapping the augmented state vector to observation space and $\epsilon_i \in \mathbb{R}^{r_i}$ represents the observation errors. These errors are usually assumed to be unbiased, Gaussian and serially uncorrelated with known covariance matrices $\mathbf{R}_i$.

We assumer that at time t_0 we have an initial estimate to the augmented state, usually referred to as the background vector denoted $\mathbf{x}^b$. This background is assumed to have unbiased, Gaussian errors with known covariance matrix $\mathbf{B}$. In 4D-Var we aim to find the initial state that minimises the wighted least squares distance to the background while minimising the weighted least squares distance of the model trajectory to the observations over the time window $t_0, \ldots, t_N$ [Lawless et al., 2013]. We do this by finding the state $\mathbf{x}_0^a$ at time t_0 that minimises the cost function

$$J(\mathbf{x}_0) = \frac{1}{2}(\mathbf{x}_0 - \mathbf{x}^b)^T \mathbf{B}^{-1}(\mathbf{x}_0 - \mathbf{x}^b) + \frac{1}{2}\sum_{i=0}^{N}(\mathbf{y}_i - \mathbf{h}_i(\mathbf{x}_i))^T \mathbf{R}_i^{-1}(\mathbf{y}_i - \mathbf{h}_i(\mathbf{x}_i)), \tag{14}$$

subject to the augmented states $\mathbf{x}_i$ satisfying the nonlinear dynamical model (11). The state that minimises the cost function, $\mathbf{x}_0^a$, is commonly called the analysis. This state is found using a minimisation routine that takes as its input arguments the cost function, the background vector ($\mathbf{x}^b$) and also the gradient of the cost function given as,

$$\nabla J(\mathbf{x}_0) = \mathbf{B}^{-1}(\mathbf{x}_0 - \mathbf{x}^b) - \sum_{i=0}^{N} \mathbf{M}_{i,0}^T \mathbf{H}_i^T \mathbf{R}_i^{-1}(\mathbf{y}_i - \mathbf{h}_i(\mathbf{x}_i)) \tag{15}$$

where $\mathbf{H}_i = \frac{\partial \mathbf{h}_i(\mathbf{x}_i)}{\partial \mathbf{x}_i}$ is our linearized observation operator and $\mathbf{M}_{i,0} = \mathbf{M}_{i-1}\mathbf{M}_{i-2}\cdots\mathbf{M}_0$ is the tangent linear model with $\mathbf{M}_i = \frac{\partial \mathbf{m}_{i-1 \to i}(\mathbf{x}_i)}{\partial \mathbf{x}_i}$. In practice $\nabla J(\mathbf{x}_0)$ is calculated using the method of Lagrange multipliers as shown in Lawless et al. [2013]. We can rewrite the cost function and its gradient to avoid the sum notation as,

$$J(\mathbf{x}_0) = \frac{1}{2}(\mathbf{x}_0 - \mathbf{x}^b)^T \mathbf{B}^{-1}(\mathbf{x}_0 - \mathbf{x}^b) + \frac{1}{2}(\hat{\mathbf{y}} - \hat{\mathbf{h}}(\mathbf{x}_0))^T \hat{\mathbf{R}}^{-1}(\hat{\mathbf{y}} - \hat{\mathbf{h}}(\mathbf{x}_0)) \tag{16}$$

and

$$\nabla J(\mathbf{x}_0) = \mathbf{B}^{-1}(\mathbf{x}_0 - \mathbf{x}^b) - \hat{\mathbf{H}}^T \hat{\mathbf{R}}^{-1}(\hat{\mathbf{y}} - \hat{\mathbf{h}}(\mathbf{x}_0)), \tag{17}$$

where,

$$\hat{\mathbf{y}} = \begin{pmatrix} \mathbf{y}_0 \\ \mathbf{y}_1 \\ \vdots \\ \mathbf{y}_N \end{pmatrix}, \ \hat{\mathbf{h}}(\mathbf{x}_0) = \begin{pmatrix} \mathbf{h}_0(\mathbf{x}_0) \\ \mathbf{h}_1(\mathbf{m}_{0\to 1}(\mathbf{x}_0)) \\ \vdots \\ \mathbf{h}_N(\mathbf{m}_{0\to N}(\mathbf{x}_0)) \end{pmatrix}, \ \hat{\mathbf{R}} = \begin{pmatrix} \mathbf{R}_{0,0} & \mathbf{R}_{0,1} & \dots & \mathbf{R}_{0,N} \\ \mathbf{R}_{1,0} & \mathbf{R}_{1,1} & \dots & \mathbf{R}_{1,N} \\ \vdots & \vdots & \ddots & \vdots \\ \mathbf{R}_{N,0} & \mathbf{R}_{N,1} & \dots & \mathbf{R}_{N,N} \end{pmatrix} \ \text{and} \ \hat{\mathbf{H}} = \begin{pmatrix} \mathbf{H}_0 \\ \mathbf{H}_1 \mathbf{M}_0 \\ \vdots \\ \mathbf{H}_N \mathbf{M}_{N,0} \end{pmatrix}. \tag{18}$$

Solving the cost function in this form also allows us to build serial time correlations into the observation error covariance matrix $\hat{\mathbf{R}}$. The off-diagonal blocks of $\hat{\mathbf{R}}$ represent correlations in time between assimilated observations and are usually taken to be zero, in section 2.6 we show how these off-diagonal blocks can be specified.

2.4 Implementation and testing of 4D-Var system

In our DALEC2 4D-Var scheme we are performing joint parameter and state estimation. The augmented state vector, $\mathbf{x}_0$, corresponds to the vector of the 17 model parameters and 6 initial carbon pool values, which can be found in the appendix in table 3. Here the nonlinear model (DALEC2) only updates the initial carbon pool values when evolving the augmented state vector forward in time with the parameters being held constant. To find the background estimate, $\mathbf{x}_b$, to the augmented state vector we can either use a previous DALEC2 model forecast's estimate of the state of the system for the site (when available) or use expert elicitation to define likely state and parameter values and ranges for the site. The background vector ($\mathbf{x}_b$) and its corresponding standard deviations (see table 3) used in this paper were provided from existing runs of the the CARbon DAta-MOdel fraMework (CARDAMOM) [Exbrayat et al., 2015]. This is a dataset derived from satellite observations of leaf area index which provides a reasonable first guess to DALEC2 state and parameter values for the Alice Holt research site. In this paper we assimilate observations of daily NEE. From Richardson et al. [2008] the measurement error in observations of daily NEE is between 0.2 to 0.8gCm^{-2}day^{-1}. We assume a variance of 0.5gCm^{-2}day^{-1} in our assimilated observations of daily NEE as we found this variance gave the best weighting to the observations in the assimilation algorithm, producing the best results for our forecast of NEE after assimilation.

In order to find the tangent linear model (TLM) for DALEC2 it is necessary to find the derivative of the model at each time step with respect to the 17 model parameters and the 6 carbon pools. We use the AlgoPy automatic differentiation package [Walter and Lehmann, 2013] in Python to calculate the TLM at each time step. This package uses forward mode automatic differentiation to calculate the derivative of our model. In the following tests we use a diagonal approximation to our background and observational error covariance matrices so that, $\mathbf{B}_{diag} = \text{diag}(\boldsymbol{\sigma}_b)^2$ and $\hat{\mathbf{R}}_{diag} = \text{diag}(\boldsymbol{\sigma}_o)^2$, where $\boldsymbol{\sigma}_b$ is the vector of background standard deviations found in table 3 and $\boldsymbol{\sigma}_o$ is the vector of observational standard deviations, for a single observation of NEE $\sigma_o^2 = 0.5$gCm^{-2}day^{-1}. The minimisation routine used in our data assimilation experiments is the truncated Newton method [Nocedal and Wright, 1999] from the Python package Scipy.optimize [Jones et al., 2001]. In sections 2.4.1 to 2.4.3 we show tests of our scheme.

2.4.1 Test of tangent linear model

We can have confidence that our implementation of the TLM for DALEC2 is correct as it passes the following relevant tests [Li et al., 1994]. In 4D-Var we assume the tangent linear hypothesis,

$$\mathbf{m}_{0\to i}(\mathbf{x}_0 + \gamma\delta\mathbf{x}_0) \approx \mathbf{m}_{0\to i}(\mathbf{x}_0) + \gamma\mathbf{M}_{i,0}\delta\mathbf{x}_0, \tag{19}$$

where $\delta\mathbf{x}_0$ is a perturbation of the initial augmented state $\mathbf{x}_0$ and γ is a parameter controlling the size of this perturbation. The validity of this assumption depends on how nonlinear the model is, the length of the assimilation window and the size of the augmented state perturbation $\delta\mathbf{x}_0$. We can test this by rearranging equation (19) to find,

$$\frac{||\mathbf{m}_{0\to i}(\mathbf{x}_0 + \gamma\delta\mathbf{x}_0) - \mathbf{m}_{0\to i}(\mathbf{x}_0)||}{||\gamma\mathbf{M}_{i,0}\delta\mathbf{x}_0||} \to 0, \tag{20}$$

as $\gamma \to 0$ (here we are using the Euclidean norm). Figure 2 shows equation (20) plotted for DALEC2 with i fixed at 731 days, a fixed 5% perturbation $\delta\mathbf{x}_0$ and values of γ approaching zero . Figure 2 shows that the TLM behaves as expected for values of γ approaching 0. This was also tested for different choices of $\mathbf{x}_0$ and sizes of perturbation with similar results.
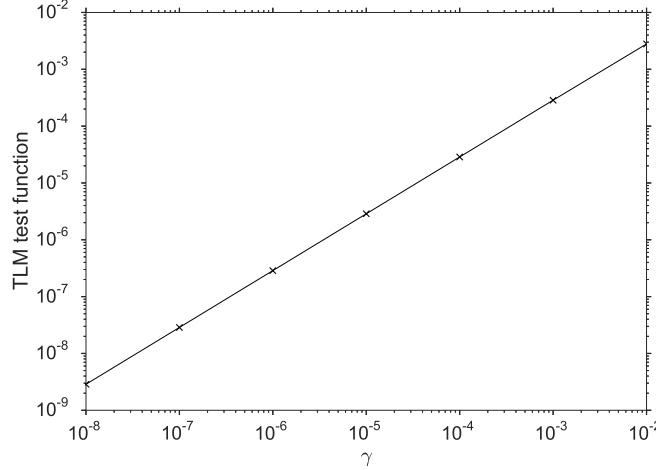

Figure 2: Plot of the tangent linear model test function (equation (20)) for DALEC2, for a TLM evolving our state 731 days forward in time and a fixed 5% perturbation, $\delta\mathbf{x}_0$.

It is also useful to show how our TLM behaves over a time window to see how the error in the TLM grows as we evolve our augmented state further forward in time. We again rearrange equation (19) with an additional error term to find,

$$\text{percentage error in TLM} = \frac{||m_{0\to i}(\mathbf{x}_0 + \gamma\delta\mathbf{x}_0) - m_{0\to i}(\mathbf{x}_0) - \gamma\mathbf{M}_{i,0}\delta\mathbf{x}_0||}{||\gamma\mathbf{M}_{i,0}\delta\mathbf{x}_0||} \times 100. \tag{21}$$

In figure 3 we can see that our TLM for DALEC2 performs well after being run forward a year with less than a 7% error for all values of $\delta\mathbf{x}_0$. By the second year we see some peaks in our error in spring and autumn. This is due to leaf on and leaf off functions in the TLM going out of phase with the nonlinear DALEC2. At these peaks the error reaches a maximum at 35% then coming back to around 10% before growing again in the autumn. For this reason we present results using a one year assimilation window in this paper.
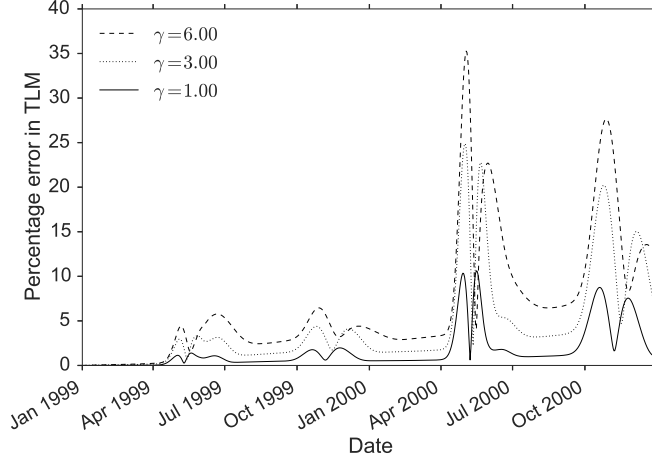
Figure 3: Plot of the percentage error in the tangent linear model (equation (21)) for DALEC2 when evolving the model state forward over a period of two years with three different values of γ and a fixed 5% perturbation $\delta\mathbf{x}_0$.

2.4.2 Test of adjoint model

The adjoint model we have implemented for DALEC2 passes correctness tests. For our TLM $\mathbf{M}_{i,0}$ and its adjoint $\mathbf{M}_{i,0}^T$ we have the identity

$$< \mathbf{M}_{i,0}\delta\mathbf{x}_0, \mathbf{M}_{i,0}\delta\mathbf{x}_0 >=< \delta\mathbf{x}_0, \mathbf{M}_{i,0}^T\mathbf{M}_{i,0}\delta\mathbf{x}_0 > \tag{22}$$

for any inner product $<,>$ and perturbation $\delta\mathbf{x}_0$. This is derived from the adjoint identity [Lawless et al., 2013]. Using the Euclidean inner product, equation (22) is equivalent to

$$(\mathbf{M}_{i,0}\delta\mathbf{x}_0)^T(\mathbf{M}_{i,0}\delta\mathbf{x}_0) = \delta\mathbf{x}_0^T(\mathbf{M}_{i,0}^T(\mathbf{M}_{i,0}\delta\mathbf{x}_0)). \tag{23}$$

We evaluated the left hand side and right hand side of this identity for differing values of $\mathbf{x}_0$ and size of perturbation $\delta\mathbf{x}_0$ and showed that they were equal to machine precision.

2.4.3 Gradient test

The 4D-Var system we have developed passes tests for the gradient of the cost function [Navon et al., 1992]. In the implementation of the cost function and its gradient we regularise the problem using a variable transform [Freitag et al., 2010]. For our cost function J and its gradient ∇J we can show that we have implemented ∇J correctly using the identity,

$$f(\alpha) = \frac{|J(\mathbf{x}_0 + \alpha\mathbf{b}) - J(\mathbf{x}_0)|}{\alpha\mathbf{b}^T\nabla J(\mathbf{x}_0)} = 1 + O(\alpha), \tag{24}$$

where $\mathbf{b}$ is a vector of unit length and α is a parameter controlling the size of $\mathbf{b}$. For small values of α not too close to machine precision we should have $f(\alpha)$ close to 1. Figure 4a shows $f(\alpha)$ for a 365 day assimilation window with $\mathbf{b} = \mathbf{x}_0||\mathbf{x}_0||^{-1}$, we can see that $f(\alpha) \to 1$ as $\alpha \to 0$, as expected until $f(\alpha)$ gets too close to machine zero at $O(\alpha) = 10^{-11}$. This was also tested with $\mathbf{b}$ in different different directions and similar results obtained.

We can also plot $|f(\alpha) - 1|$, where we expect $|f(\alpha) - 1| \to 0$ as $\alpha \to 0$. In figure 4b we have plotted $|f(\alpha) - 1|$ for the same conditions as in figure 4a, we can see that $|f(\alpha) - 1| \to 0$ as $\alpha \to 0$, as expected (before $|f(\alpha) - 1|$ gets too close to machine precision at $O(\alpha) = 10^{-8}$). This gives us confidence that the gradient of our cost function is implemented correctly.
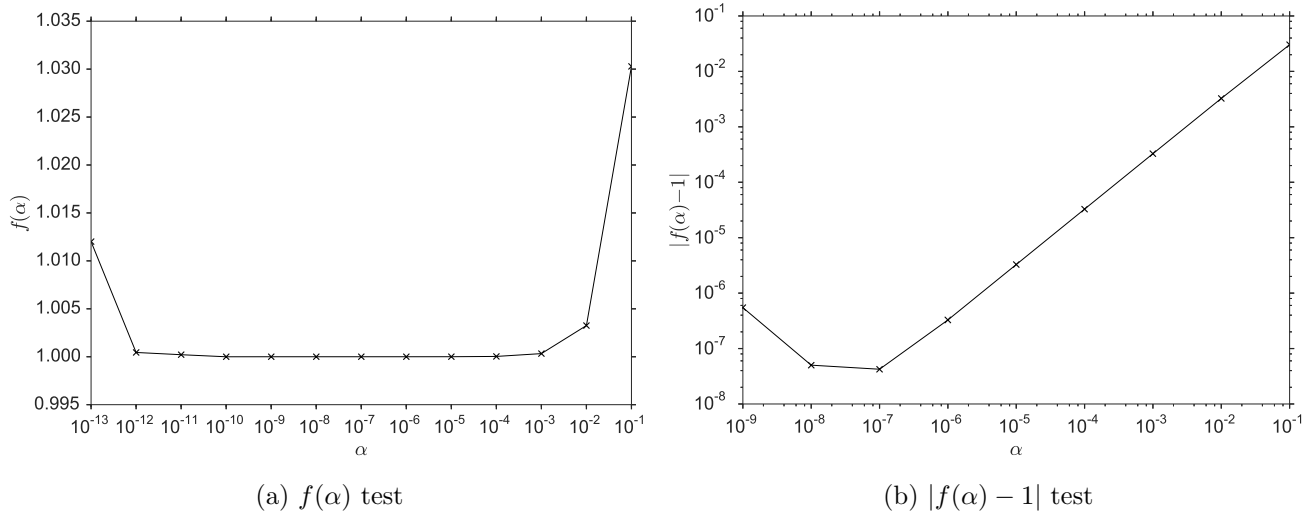
(a) $f(\alpha)$ test (b) $|f(\alpha) - 1|$ test

Figure 4: Tests of the gradient of the cost function for a 365 day assimilation window with $\mathbf{b} = \mathbf{x}_0 ||\mathbf{x}_0||^{-1}$.

2.5 Including correlations in the background error covariance matrix

As discussed in section 1, including correlations in $\mathbf{B}$ impacts how information from assimilated observations is spread between different types of analysis variables [Bannister, 2008]. We explored a number of different methods in order to include parameter-state correlations in $\mathbf{B}$. In this paper we present a method using a set of ecological dynamical constraints, based on expert judgement, on model parameters and state variables from Bloom and Williams [2015]. Bloom and Williams [2015] show that implementing these constraints in a Metropolis Hastings MCMC data assimilation routine improves results significantly. The constraints impose conditions on carbon pool turnover and allocation ratios, steady state proximity and growth and decay of model carbon pools.

In order to create a correlated background error covariance matrix, $\mathbf{B}_{corr}$, using these constraints we create an ensemble of state vectors which we then take the covariance of to give us $\mathbf{B}_{corr}$. To create this ensemble we use the following procedure:

1. Draw a random augmented state vector, $\mathbf{x}_i$, from the multivariate truncated normal distribution described by

$$\mathbf{X} \sim \mathcal{N}(\mathbf{x}^b, \mathbf{B}_{diag}), \tag{25}$$

   where $\mathbf{B}_{diag}$ is the diagonal matrix described in section 2.4 and $\mathbf{X}$ is bound by the parameter and state ranges given in table 3 in the appendix.

2. Test this $\mathbf{x}_i$ with the ecological dynamical constraints (requiring us to run the DALEC2 model using this state).

3. If $\mathbf{x}_i$ passes it is added to to our ensemble, else it is discarded.

Once we have a full ensemble we then take the covariance of the ensemble to find $\mathbf{B}_{corr}$. We chose an ensemble size of 1500 as using a larger ensemble did not appear to change values of correlations significantly. In figure 5 we have plotted the correlation matrix or normalised error covariance matrix associated with $\mathbf{B}_{corr}$. This matrix includes both positive and negative correlations between parameter and state variables, with correlations of 1 down the diagonal between variables of the same quantity as expected. The largest positive off-diagonal correlation is 0.42 between f_{lab} and C_{lab}. This makes physical sense as f_{lab} is the parameter controlling the amount of GPP allocated to the labile carbon pool, C_{lab}.
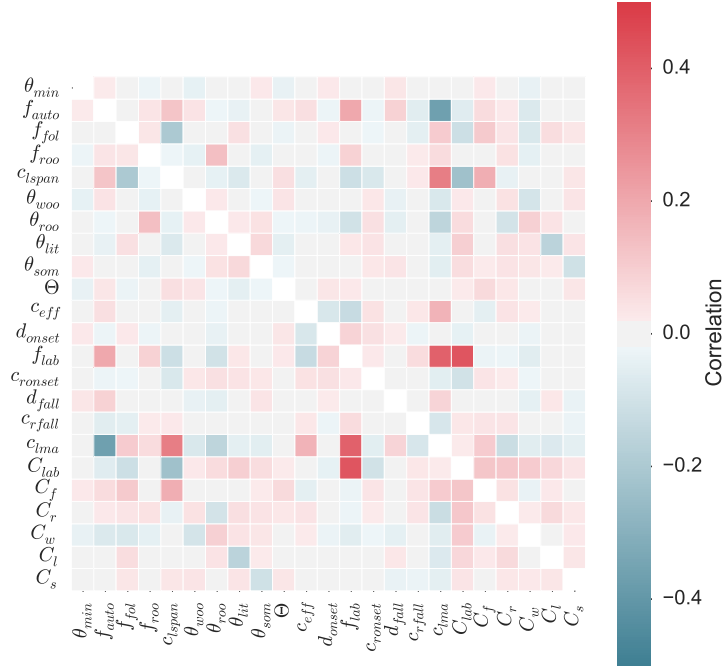
Figure 5: Background error correlation matrix created using method in section 2.5. Here the correlation scale for off-diagonal values ranges from -0.5 to 0.5 with the correlation along the diagonal being 1. For explanation of parameter and state variable symbols see table 3.

2.6 Specifying serial correlations in the observation error covariance matrix

The observation error covariance matrix does not only represent the instrumentation error for an observation but also the error in the observation operator (mapping the model state to the observation) and representativity error (error arising from the model being unable resolve the spatial and temporal scales of the observations). These other sources of error represented in $\hat{\mathbf{R}}$ can also lead to correlations between observation errors [Waller et al., 2014]. Errors in NEE observations come from different sources such as instrument errors, sampled ecosystem structure from the variable footprint of the flux tower and turbulent conditions (when we have low turbulence and limited air mixing NEE is underestimated). These errors due to turbulence can still have effect even after u^* filtering [Papale et al., 2006]. Due to this dependence on atmospheric conditions we expect the errors in observations of NEE to be serially correlated, as the atmospheric signal itself is serially correlated [Daley, 1992]. If we were assimilating half hourly observations of NEE we would expect stronger correlations between observation errors, as atmospheric conditions are more constant at this time scale, with correlations between observation errors getting weaker with lower frequency observations. Although some studies suggest that the correlation between NEE measurement errors on the scale of a day is negligible [Lasslop et al., 2008], It is also likely that error in the observation operator and representativity error will lead to observation error correlations for NEE [Waller et al., 2014].

In section 2.3 we have re-written the 4D-Var cost function in equation (16) in order to allow the specification of serial observation error correlations in our assimilation scheme. These serial correlations are represented by the off-diagonal blocks of $\hat{\mathbf{R}}$. In work carried out with spatial correlations it has been shown that the structure of the correlation is not critical and that it is better to include some estimate of error correlation structure in the observation error covariance matrix than wrongly assume that errors are independent [Healy and White, 2005, Stewart et al., 2013]. As a first attempt we try including temporal correlations on the scale of the observation frequency. We adapt the simple Gaussian model found in Järvinen et al. [1999] (a second order autoregressive correlation function was also tested but is

not presented here). The correlation r between 2 observations at times t_1 and t_2 is given as,

$$r = \begin{cases} a\exp\left[\frac{-(t_1-t_2)^2}{\tau^2}\right] + (1-a)\delta_{t_1-t_2} & |t_1-t_2| \leq \eta \\ 0 & \eta < |t_1-t_2| \end{cases},$$ (26)

where τ is the e-folding time, a controls the strength of correlation, δ is the Kronecker delta and η is the cut off time after which the correlation between two observation errors is zero. We have incorporated a cut off for correlations between observation errors as the assumed correlation length scale for our assimilated observations is short. This cut off along with the form of correlation function using the Kronecker delta helps ensure $\hat{\mathbf{R}}$ is positive definite and therefore invertible, as required in the assimilation process. The variance assumed in the observations of NEE is $0.5\text{gCm}^{-2}\text{day}^{-1}$ as described in section 2.4.
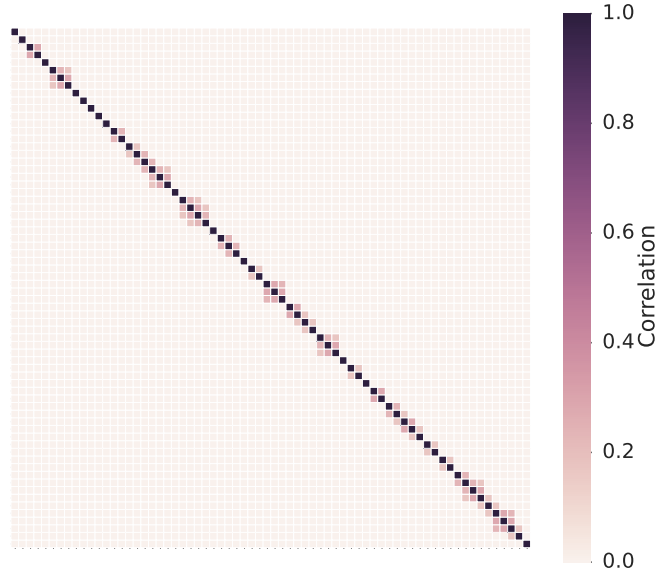
Figure 6: Observation error correlation matrix for the 67 observations used in assimilation created using method in section 2.6 with $\tau = 4$, $a = 0.3$ and $\eta = 4$.

Figure 6 shows the correlation matrix for $\hat{\mathbf{R}}$ created using equation (26). There are 67 NEE observations in this one year assimilation window, these observations are not all on adjacent days and this is evident in the structure of $\hat{\mathbf{R}}$. The effect of the short e-folding time chosen here ($\tau = 4$) provides the desired structure.

3 Results

3.1 Experiments

In the following sections we present the results of four experiments where we vary the representations of $\mathbf{B}$ and $\hat{\mathbf{R}}$ while assimilating the same NEE observations in the window from the beginning of January 1999 to the end of December 1999. As shown in figure 3 the performance of the tangent linear model deteriorates after the first year. We then forecast the NEE over the next 14 years (Jan 2000 - Dec 2013) and compare with the observed data. Using this shorter analysis window with a long forecast allows us to see the effect of including correlations in the error statistics more clearly. These experiments are outlined in table 1 where $\mathbf{B}_{diag}$ and $\hat{\mathbf{R}}_{diag}$ are the diagonal matrices of the parameter and state variances and the observations variances respectively and $\mathbf{B}_{corr}$ and $\hat{\mathbf{R}}_{corr}$ are the matrices as specified in section 2.5 and section 2.6 respectively.

Experiment	$\mathbf{B}_{diag}$	$\hat{\mathbf{R}}_{diag}$	$\mathbf{B}_{corr}$	$\hat{\mathbf{R}}_{corr}$
A	×	×		
B		×	×	
C	×			×
D			×	×

Table 1: The combination of error covariance matrices used in each data assimilation experiment.

3.2 Experiment A

In this experiment $\mathbf{B}_{diag}$ and $\hat{\mathbf{R}}_{diag}$ were used in our assimilation as described in section 3.1. Because these contain no correlations this experiment forms the baseline by which the subsequent results from assimilation experiments are judged.

Figure 7a shows assimilation and forecast results for NEE. We can see that assimilating the observations of NEE has improved the background with our analysis trajectory (green line) fitting well with the observations during the assimilation window (Jan 1999- Dec 1999). The analysis trajectory then diverges in the forecast (Jan 2000 - Dec 2013). This can be seen more clearly in figue 8a, where we have an over prediction of respiration in the winter and the seasonal cycle does not match that of the observations.

To see how well our forecast performs after assimilation we show a scatter plot of modelled NEE against observed NEE in figure 9b. From table 2 the predictions have a Root-Mean-Square Error (RMSE) of 4.22gCm^{-2} and a bias of -0.3gCm^{-2} for our forecast of NEE, whereas our analysis (Jan 1999 - Dec 1999) has a RMSE of 1.36gCm^{-2} and a bias of -0.03gCm^{-2}. The background trajectory meanwhile has a RMSE of 3.86gCm^{-2} and a bias of -1.60gCm^{-2} in the analysis window (Jan 1999 - Dec 1999) and the same RMSE of 3.86gCm^{-2} but a bias of -1.36gCm^{-2} during the forecast period (Jan 2000 - Dec 2013). Although using $\mathbf{B}_{diag}$ and $\hat{\mathbf{R}}_{diag}$ in the assimilation has considerably reduced the RMSE in the analysis period, it has also increased the RMSE in the forecast of NEE. However it has reduced the bias in the model forecast considerably from -1.36gCm^{-2} to -0.3gCm^{-2}. The bias in the background is due to the background model less negative values of NEE than observed (i.e. above the 1:1 line shown in figure 9a). This leads to considerably worse results for the background trajectory than our analysis and its forecast for total forest carbon uptake.

3.3 Experiment B

Here $\mathbf{B}_{corr}$ (as defined in section 2.5) and $\hat{\mathbf{R}}_{diag}$ are used in the assimilation. Figure 7b shows assimilation and forecast results for NEE. In figure 8b we can see that the forecast performs considerably better than in experiment A, with the analysis trajectory no longer over predicting winter respiration and matching the observed seasonal cycle of NEE more closely in the forecast period (Jan 2000 - Dec 2013). From figure 9c and table 2 we see that the forecast RMSE has almost halved (now 2.56gCm^{-2}) with a reduction in bias also, now -0.2gCm^{-2}. In comparison using $\mathbf{B}_{corr}$ in our assimilation very slightly degrades the fit for the analysis (Jan 1999 - Dec 1999), with a RMSE of 1.42gCm^{-2} and a bias of -0.04gCm^{-2}, as shown in table 2.

As discussed in section 1 previous work has shown the importance of specifying parameter-state correlations when using variational data assimilation for joint parameter-state estimation [Smith et al., 2009]. Although in 4D-Var some correlation structure is added implicitly as $\mathbf{B}_{diag}$ is evolved through time in experiment A, observations near the beginning of the window (before significant correlations develop in $\mathbf{B}_{diag}$) will not be spread in a multivariate way. The correlations developed by the implicit evolution of $\mathbf{B}_{diag}$ may also not include important physical relationships between variables. Therefore by not specifying these correlations in experiment A we allow our parameter and state variables to attain unrealistic values in order to find the best fit to the observations in the analysis window (Jan 1999 - Dec

1999), leading to the divergence seen in the forecast (1999-2014) in experiment A.

We can see the effect that including correlations in $\mathbf{B}$ has on the analysis update in figure 10. For some variables including correlations in $\mathbf{B}$ has had a large impact on the analysis update after assimilation. This is particularly clear for the f_{lab} parameter. The largest positive off-diagonal correlation in $\mathbf{B}_{corr}$ is between C_{lab} and f_{lab}, with f_{lab} also having a large positive correlation with c_{lma} as shown in section 2.5. The effect of these correlations has been to change the analysis increment for f_{lab} from being slightly positive in experiment A to being strongly negative by following the analysis update of its correlated variables C_{lab} and c_{lma}. From figure 10 we can also see some of the reasons for the improved fit to the observations in experiment B. We see that the parameters controlling day of leaf on (d_{onset}) has been updated differently in comparison to experiment A, with day of leaf on now being later in the year, again this is due to the included correlations in $\mathbf{B}$. This allows the forecast to better match the observed seasonal cycle of NEE. The forecast is also no longer over predicting winter respiration as in experiment A. From figure 10 we see that the main parameters controlling ecosystem respiration in NEE (f_{auto}, θ_{lit}, θ_{som}, Θ) have been reduced in comparison with experiment A, leading to an improved fit to observations in experiment B. In experiment A we also had an over prediction of peak carbon uptake in summer which has been improved in this experiment. From figure 10 we see that one of the parameters controlling the magnitude of gross primary productivity (c_{eff}) has been decreased in comparison to experiment A. This leads to less extreme predictions of peak summer carbon uptake than in experiment A.

The added constraint provided by the correlations in $\mathbf{B}_{corr}$ reduces the likelihood that parameter and state variables will attain unrealistic values in order to fit the assimilated observations. Although this has led to a slightly degraded fit to the observations in the analysis window (Jan 1999 - Dec 1999) it has also significantly improved the fit to observations for the forecast (Jan 2000 - Dec 2013).

3.4   Experiment C

Here we use $\mathbf{B}_{diag}$ and $\hat{\mathbf{R}}_{corr}$ (as defined in section 2.6) in the assimilation. Results shown in figure 7c and 8c appear similar to those in section 3.2 however there are some differences. From table 2 and figure 9d we see a slight reduction in RMSE for our forecast (now 4.09gCm^{-2}) in comparison with experiment A. As in experiment B the fit to the observations in the analysis window (Jan 1999 - Dec 1999) is very slightly degraded as the added correlations in $\hat{\mathbf{R}}_{corr}$ act to reduce the weight of the observations in the assimilation [Järvinen et al., 1999]. The changes seen when using $\hat{\mathbf{R}}_{corr}$ in the assimilation are less than when using $\mathbf{B}_{corr}$ as the correlations specified in $\hat{\mathbf{R}}_{corr}$ are on a short timescale and smaller than those in $\mathbf{B}_{corr}$. In figure 10 we can see that the changes between experiment A and C in the analysis increment are much less than when using $\mathbf{B}_{corr}$.

We also expect that specifying time correlations in $\hat{\mathbf{R}}$ will help when assimilating other less frequently sampled data streams along with NEE as the serial correlations reduce the weight given to the mean of the more frequently sampled observations (here NEE) and also reduce the information content of these more frequently sampled observations [Daley, 1992, Järvinen et al., 1999], meaning that less frequently sampled data streams can have more impact on the assimilation.

3.5   Experiment D

In the final experiment we use $\mathbf{B}_{corr}$ and $\hat{\mathbf{R}}_{corr}$ in the assimilation. Figure 8d and figure 8b shows that using both correlated matrices gives similar results as experiment B when $\mathbf{B}_{corr}$ is used with $\hat{\mathbf{R}}_{diag}$. However using $\hat{\mathbf{R}}_{corr}$ in addition to $\mathbf{B}_{corr}$ provides similar improvements as in experiment C. From table 2 and figure 9e we see the forecast RMSE is slightly reduced again still from results in experiment B to 2.38gCm^{-2}. Using both matrices appears to combine the beneficial effects described in both section 3.3 and section 3.4. In figure 10 we can see that the analysis increment is very similar to experiment B.

(a) Experiment A

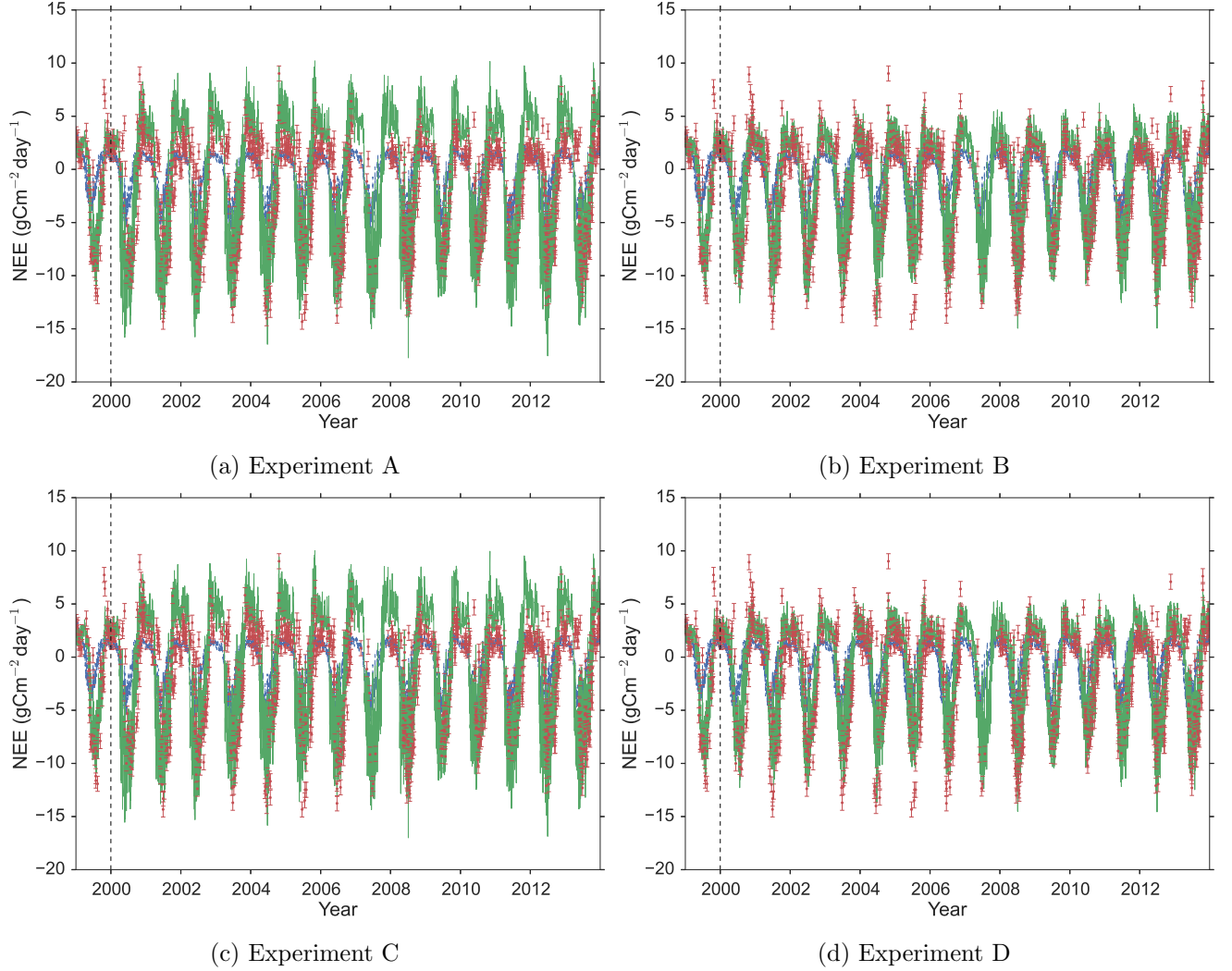(b) Experiment B

(c) Experiment C

(d) Experiment D

Figure 7: One year assimilation and fourteen year forecast of Alice Holt NEE with DALEC2, blue dotted line: background model trajectory, green line: analysis and forecast after assimilation, red dots: observations from Alice Holt flux site with error bars.
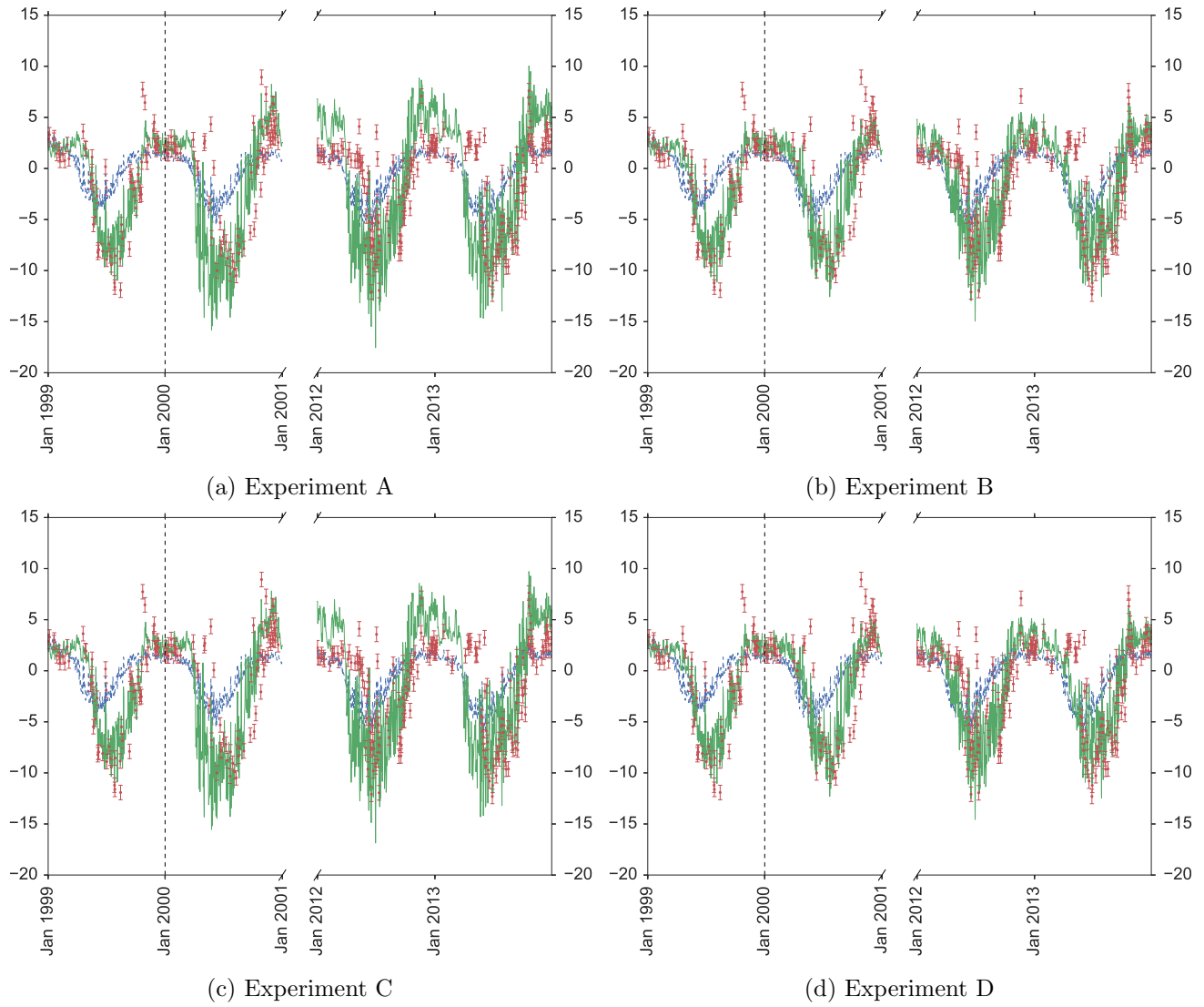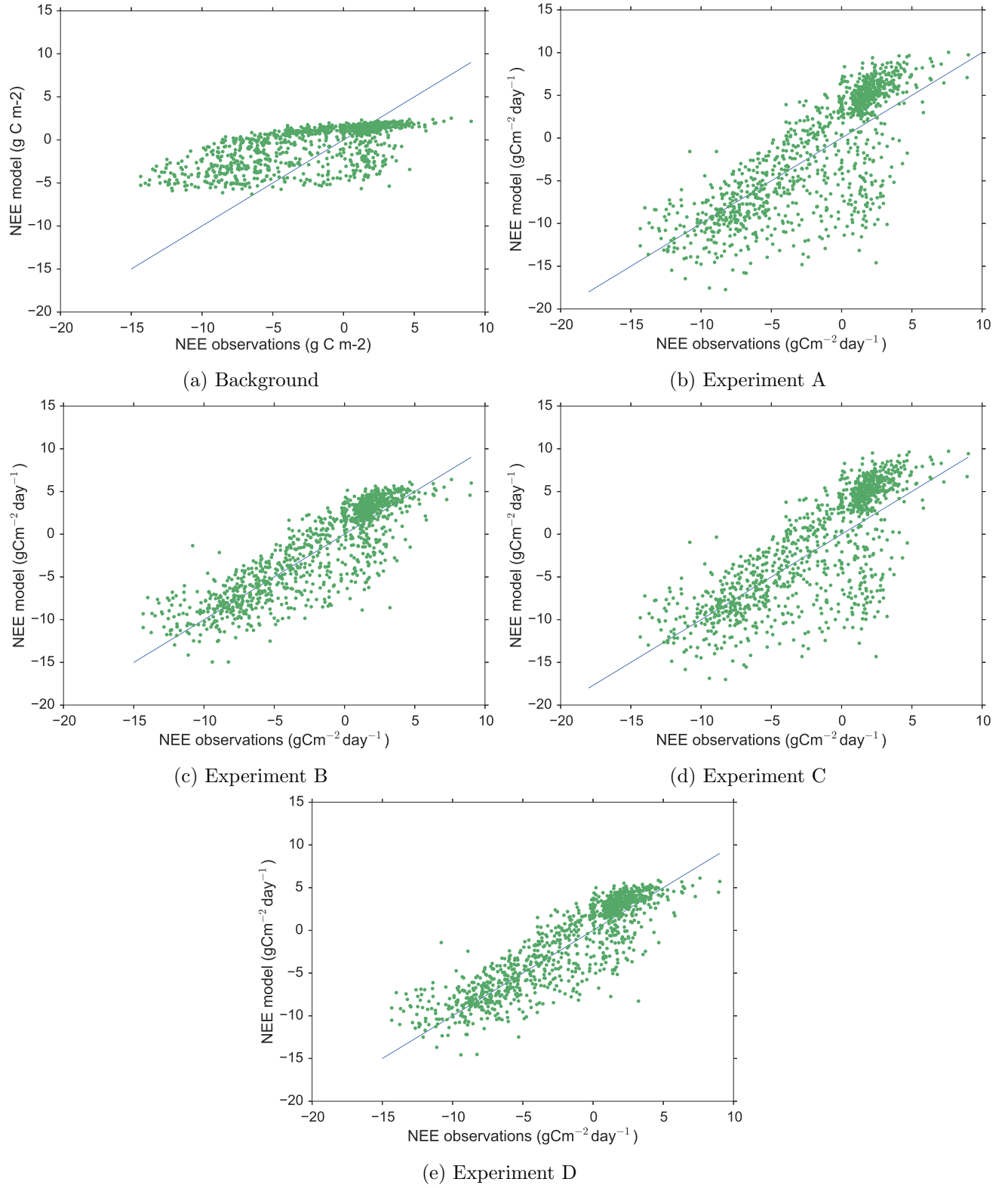
(a) Experiment A

(b) Experiment B

(c) Experiment C

(d) Experiment D

Figure 8: As figure 7 but only showing the first and final two years results from the one year assimilation and fourteen year forecast of Alice Holt NEE with DALEC2, blue dotted line: background model trajectory, green line: analysis and forecast after assimilation, red dots: observations from Alice Holt flux site with error bars.

(a) Background

(b) Experiment A

(c) Experiment B

(d) Experiment C

(e) Experiment D

Figure 9: Forecast scatter plot of modelled daily NEE vs. observations for Jan 2000 - Dec 2013 (green dots). Blue line represents the 1-1 line.
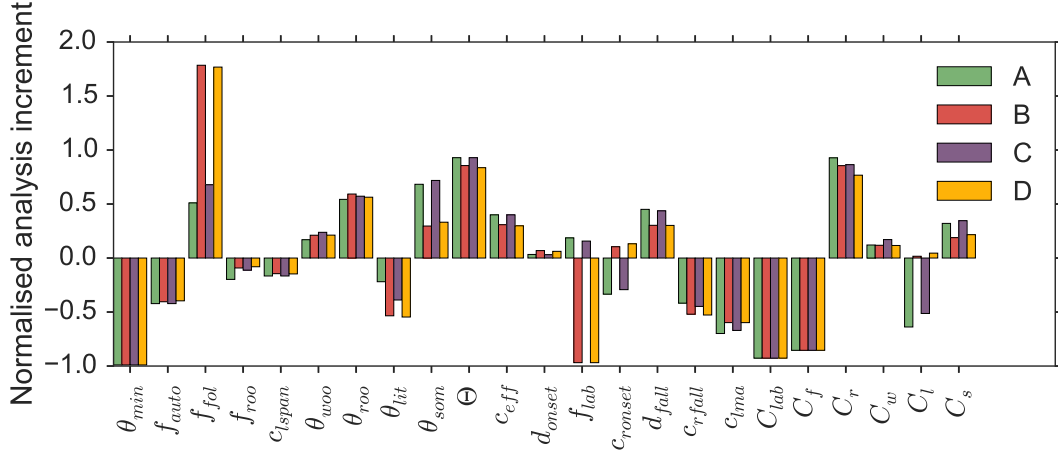
Figure 10: Normalised analysis increment $\left(\frac{(\mathbf{x}_a - \mathbf{x}_b)}{\mathbf{x}_b}\right)$ for the four experiments. Explanation of parameter and state variable symbols in table 3.

3.6   Summary

In our experiments we have shown that both $\mathbf{B}_{corr}$ and $\hat{\mathbf{R}}_{corr}$ have the effect of improving the model forecast of NEE. As it can be difficult to inspect the skill of a certain model by only plotting model trajectories, in figure 11 we show Taylor diagrams displaying a statistical comparison of the four experiment and background analysis (Jan 1999 - Dec 1999) and forecast (Jan 2000 - Dec 2013) results with the observations of NEE. Here the radial distances from the origin to the points are proportional to the pattern standard deviations and the azimuthal positions give the correlation coefficient between the modelled and observed NEE [Taylor, 2001]. If a model predicted the observations perfectly it would have a correlation coefficient of 1 and a radial distance matching that of the observations (represented by the dotted line). Figure 11a shows that all the experiments give very similar results in the analysis window (Jan 1999 - Dec 1999) with all the experiment points closely grouped on top of each other, whereas figure 11b shows the significant difference between the experiment results in the forecast (Jan 2000 - Dec 2013).

Analysis (Jan 1999 - Dec 1999)		
Experiment	RMSE (gCm^{-2})	Bias (gCm^{-2})	Correlation coefficient
Background	3.86	-1.60	0.70
A	1.36	-0.03	0.96
B	1.42	-0.04	0.95
C	1.37	-0.09	0.96
D	1.43	-0.09	0.95
Forecast (Jan 2000 - Dec 2013)		
Experiment	RMSE (gCm^{-2})	Bias (gCm^{-2})	Correlation coefficient
Background	3.86	-1.36	0.66
A	4.22	-0.30	0.79
B	2.56	-0.20	0.87
C	4.09	-0.51	0.78
D	2.38	-0.33	0.88

Table 2: Analysis (Jan 1999 - Dec 1999) and forecast (Jan 2000 - Dec 2013) results for experiments and background when judged against observed NEE.

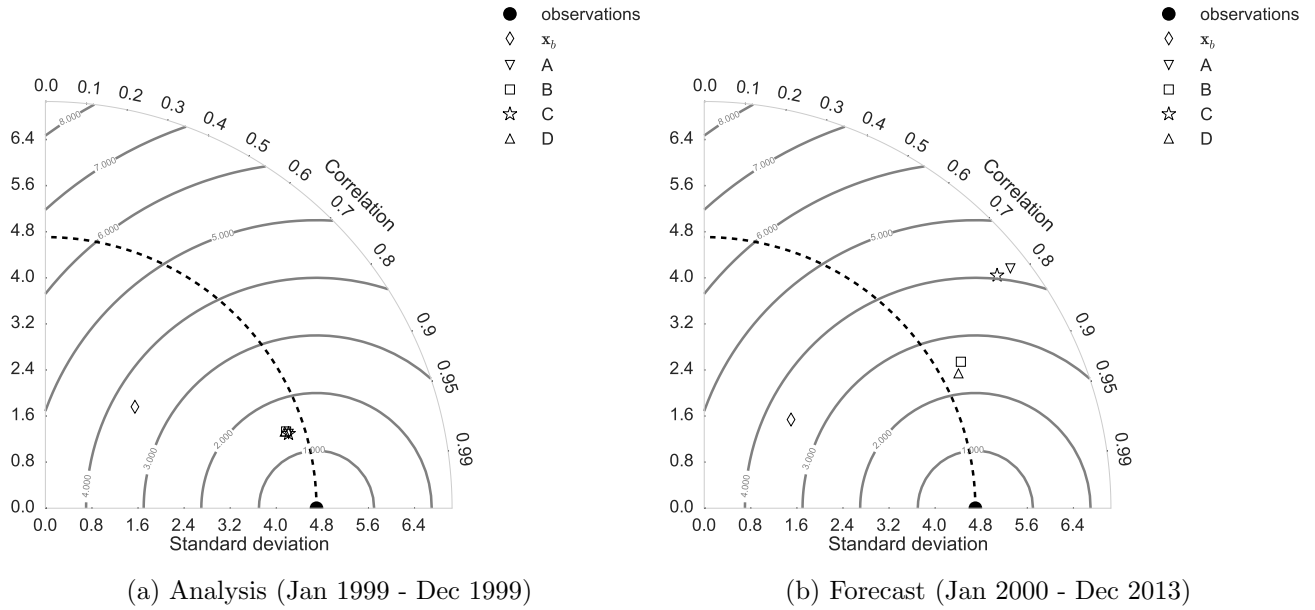(a) Analysis (Jan 1999 - Dec 1999)   (b) Forecast (Jan 2000 - Dec 2013)

Figure 11: Taylor diagrams displaying statistical comparison of the four experiment and background analysis (Jan 1999 - Dec 1999) and forecast (Jan 2000 - Dec 2013) results with observations of NEE ($gCm^{-2}day^{-1}$). The dotted line represents the standard deviation of the observations and the contours represent values of constant root mean square error between model and observations.

4 Discussion

In this paper we have implemented the DALEC2 functional ecology model in a 4D-Var data assimilation scheme, building an adjoint of the DALEC2 model and applying rigorous tests to our scheme. Using 4D-Var can provide much faster assimilation results than MCMC techniques as we have knowledge of the derivative of the model. For our experiments the 4D-Var routine has taken in the order of 10^2 function evaluations to converge to a minimum, whereas MCMC techniques using the same model take in the order of 10^8 function evaluations [Bloom and Williams, 2015]. However, we do assume that the statistics of the problem are Gaussian whereas MCMC techniques do not. We have shown that 4D-Var is a valid tool for improving the DALEC2 model estimate of NEE and that even when assimilating only a single year of NEE observations we can improve our forecast significantly. In practice this type of data assimilation routine would be run in cycling mode running the analysis from the first year as the background for the second then iterating this until all data is assimilated [Moodey et al., 2013]. However, here our aim is to investigate the effect of specifying correlations in background and observation error statistics on the forecast of NEE. We have therefore assimilated just one year of NEE observations and produced a long 14 year forecast in order to see more clearly the effect of including these correlations on our forecast when judging against observations. The observations of daily NEE from the Alice Holt flux site are quite variable year to year, peak summer uptake varies from $-14.35gCm^{-2}day^{-1}$ to $-9.04gCm^{-2}day^{-1}$, and therefore provide a reasonable test for the ability of the DALEC2 model forecast, especially over a 14 year period.

We then considered the nature of background and observation errors. The effect of specifying parameter-state correlations in our background information and serial correlations between our observation errors was explored.

The technique presented here to specify $\mathbf{B}_{corr}$ has been shown to have significantly improved forecasts of NEE over using a diagonal representation of $\mathbf{B}$. In section 3.3 we discuss how the correlations in $\mathbf{B}_{corr}$ impact the analysis update for the parameter and state variables (see figure 10) causing the seasonal cycle of carbon uptake and magnitude of fluxes to fit more closely with the observations than when using

18

a diagonal $\mathbf{B}$ in the assimilation algorithm. These results agree with those of Smith et al. [2009] where the importance of specifying parameter-state correlations when performing joint parameter and state estimation with variational data assimilation was shown. The method for specifying $\mathbf{B}_{corr}$ in this paper used a series of ecological dynamical constraints taken from Bloom and Williams [2015]. In cases where these type of constraints are not available there are other methods to build correlations into $\mathbf{B}$. One technique we also tested (not presented here) to create a correlated $\mathbf{B}$ involved evolving an ensemble of state vectors over the length of the chosen assimilation window using the model (DALEC2) and then taking the covariance of the evolved ensemble. This gave us a $\mathbf{B}$ with parameter-state and state-state correlations, but no parameter-parameter correlations as the parameters are not updated by the model. Using the $\mathbf{B}$ created with this method also improved assimilation results significantly over using a diagonal $\mathbf{B}$. A larger number of different tests were run using different background vectors and variances and it was found that specifying some form of correlation structure in $\mathbf{B}$ always made an improvement to the results of our assimilation. As this work has only considered a single deciduous site, it would be useful to apply the techniques detailed here for an evergreen site. Evergreen ecosystems usually have a less extreme seasonal variation, it will therefore be interesting to see if we have a similar improvement for evergreen ecosystem forecast results when using a $\mathbf{B}_{corr}$ created using the same method.

The purpose of this exercise was to see how well we could forecast NEE while also investigating the effect of including correlations between error statistics. It was not an attempt to recover all the parameters and state variables with a high level of accuracy. However, it is still instructive to look at these values and compare with data where available. In Meir et al. [2002] an observed range is given for leaf mass per area (c_{lma}) for the Alice Holt flux site of between 40 to 80gCm^{-2}. The background value for c_{lma} in our experiments is 128.5gCm^{-2}. When using diagonal error covariance matrices in experiment A we find a value of 38.7gCm^{-2} for c_{lma} after assimilation which is almost within the range given by Meir et al. [2002]. In experiment D when using error covariance matrices including correlations c_{lma} has a value of 51.6gCm^{-2} after assimilation, this is well within the observed range given by Meir et al. [2002] and again shows an improvement when using the correlated error covariance matrices. From observations made by Forest Research we also have estimates to the above and below ground woody carbon pool (C_{woo}) at the start of 1999 with a value of 14258gCm^{-2}. The background value for C_{woo} in our experiments is 6506gCm^{-2}. When using diagonal error covariance matrices in experiment A we find a value of 7291gCm^{-2} for C_{woo}, an increase but still far away from the observed estimate. In experiment D when using error covariance matrices including correlations C_{woo} has a value of 7262gCm^{-2} a similar result as experiment A. Here the assimilation has not been able to recover a value of C_{woo} similar to that of the observed estimate. This is expected as we are assimilating observations of daily NEE only and NEE is a product of Gross Primary Productivity (GPP) and Total ecosystem respiration (RT), (NEE = RT - GPP), with neither GPP nor RT being direct functions of C_{woo}. Therefore it is not possible to recover an accurate value of C_{woo} as our assimilated observations are not significantly impacted by large changes in this state variable (i.e. equifinality), this result is also found in Fox et al. [2009]. This also explains why we are able to recover a reasonable value of c_{lma} from the assimilation, as from equation (1) we can see that c_{lma} is one of the input arguments taken by GPP. The function calculating GPP will therefore be sensitive to variations in the c_{lma} parameter and so assimilation observations of NEE should help to constrain this parameter.

In numerical weather prediction it has been shown that including correlations in $\mathbf{R}$ can help improve data assimilation results [Stewart et al., 2013, Weston et al., 2014]. However the specified correlations have most commonly been satellite interchannel correlations with observations errors still being considered independent in time. In this paper we have shown that including correlations between observation errors in time can also improve data assimilation results, here improving the DALEC2 model forecast of NEE. We expect including these serial correlations to have an even greater impact when assimilating more than one data stream. When assimilating multiple data streams more frequently sampled observation types (such as NEE) have much more impact on the assimilation than data streams sampled less frequently. Specifying serial correlations between observations of the same type has the effect of reducing the weight

given to the mean of the observations [Järvinen et al., 1999], thus allowing less frequent data streams to have more impact on the assimilation. Using the form of $\hat{\mathbf{R}}$ given in this paper for specifying serial correlations will also allow us to specify serial correlations between different observation types. When running the DALEC2 model with a day-night time step, instead of the daily time step used for this paper, this will allow us to build in the type of correlations investigated by Baldocchi et al. [2015] between ecosystem respiration and canopy photosynthesis. More work is needed to investigate the effect of including correlations between observations error statistics when assimilating multiple data streams.

The $\hat{\mathbf{R}}_{corr}$ presented in this paper has a weak correlation ($a = 0.3$) in time between observations of NEE, this representation of $\hat{\mathbf{R}}_{corr}$ has improved the model forecast of NEE. However other choices of $\hat{\mathbf{R}}_{corr}$ (with stronger correlations between observations) tested for this paper degraded the forecast. This is probably due to the specified correlations being unrealistic and suggests a more diagnostic approach is needed for the calculation of serial correlations in $\hat{\mathbf{R}}$. One option would be to adapt the Desroziers et al. [2005] diagnostic, which has been used successfully in numerical weather prediction for diagnosing observation error correlations for observations taken at the same time [Weston et al., 2014], and extending this technique to diagnose serial correlations. This will form the basis of future work.

5   Conclusion

Functional ecology and land surface model data assimilation routines largely treat prior estimates of parameter-state uncertainties and observation error statistics as independent and uncorrelated. In this paper we have shown the importance of including estimates to such correlations, especially between background parameter and state error statistics when performing joint parameter and state estimation.

When performing joint parameter and state estimation using including correlations in the background error covariance matrix significantly improves our forecast after assimilation, in comparison to using a diagonal representation of $\mathbf{B}$. Specifying serial correlations between observation errors in $\hat{\mathbf{R}}$ also improves our forecast and we expect these correlations to have a greater impact when assimilating more than one data stream. More work is needed to investigate the effect of including these correlations when assimilating multiple data streams. The development of a more diagnostic tool for the calculation of the error correlation structure in $\hat{\mathbf{R}}$ is also important.

When including both parameter-state correlations in $\mathbf{B}$ and time correlations between observation errors in $\hat{\mathbf{R}}$ and assimilating only a single year of NEE observations we can forecast 14 years of NEE observations with a root-mean square error of $2.38 \text{gCm}^{-2}\text{day}^{-1}$ and a correlations coefficient of 0.88. This is a significant 44% reduction in error from the results when using a $\mathbf{B}$ and $\hat{\mathbf{R}}$ with no specified correlations of $4.22 \text{gCm}^{-2}\text{day}^{-1}$ and a correlation coefficient of 0.79.

6   Acknowledgements

References

C. Bacour, P. Peylin, N. MacBean, P. J. Rayner, F. Delage, F. Chevallier, M. Weiss, J. Demarty, D. Santaren, F. Baret, D. Berveiller, E. Dufrêne, and P. Prunet. Joint assimilation of eddy-covariance flux measurements and FAPAR products over temperate forests within a process-oriented biosphere model. *Journal of Geophysical Research: Biogeosciences*, pages n/a–n/a, 2015. ISSN 21698953. doi: 10.1002/2015JG002966. URL http://doi.wiley.com/10.1002/2015JG002966.

Dennis Baldocchi. Turner review no. 15.'breathing'of the terrestrial biosphere: lessons learned from a

global network of carbon dioxide flux measurement systems. *Australian Journal of Botany*, 56(1):1–26, 2008.

Dennis Baldocchi, Cove Sturtevant, and Fluxnet Contributors. Does day and night sampling reduce spurious correlation between canopy photosynthesis and ecosystem respiration? *Agricultural and Forest Meteorology*, 207:117–126, 2015. ISSN 01681923. doi: 10.1016/j.agrformet.2015.03.010. URL http://linkinghub.elsevier.com/retrieve/pii/S016819231500088X.

Ross N Bannister. A review of forecast error covariance statistics in atmospheric variational data assimilation. i: Characteristics and measurements of forecast error covariances. *Quarterly Journal of the Royal Meteorological Society*, 134(637):1951–1970, 2008.

Peter Bauer, Alan Thorpe, and Gilbert Brunet. The quiet revolution of numerical weather prediction. *Nature*, 525(7567):47–55, 2015.

A. A. Bloom and M. Williams. Constraining ecosystem carbon dynamics in a data-limited world: integrating ecological "common sense" in a modeldata fusion framework. *Biogeosciences*, 12(5):1299–1315, 2015. ISSN 1726-4189. doi: 10.5194/bg-12-1299-2015. URL http://www.biogeosciences.net/12/1299/2015/.

Massimo Bonavita, Elias Hlm, Lars Isaksen, and Mike Fisher. The evolution of the ecmwf hybrid data assimilation system. *Quarterly Journal of the Royal Meteorological Society*, pages n/a–n/a, 2015. ISSN 1477-870X. doi: 10.1002/qj.2652. URL http://dx.doi.org/10.1002/qj.2652.

Bobby H Braswell, William J Sacks, Ernst Linder, and David S Schimel. Estimating diurnal to annual ecosystem parameters by synthesis of a carbon flux model with eddy covariance net ecosystem exchange observations. *Global Change Biology*, 11(2):335–355, 2005.

Philippe Ciais, Christopher Sabine, Govindasamy Bala, Laurent Bopp, Victor Brovkin, Josep Canadell, Abha Chhabra, Ruth DeFries, James Galloway, Martin Heimann, et al. Carbon and other biogeochemical cycles. In *Climate change 2013: the physical science basis. Contribution of Working Group I to the Fifth Assessment Report of the Intergovernmental Panel on Climate Change*, pages 465–570. Cambridge University Press, 2014.

A. M. Clayton, A. C. Lorenc, and D. M. Barker. Operational implementation of a hybrid ensemble/4d-var global data assimilation system at the met office. *Quarterly Journal of the Royal Meteorological Society*, 139(675):1445–1461, 2013. ISSN 1477-870X. doi: 10.1002/qj.2054. URL http://dx.doi.org/10.1002/qj.2054.

Roger Daley. The Effect of Serially Correlated Observation and Model Error on Atmospheric Data Assimilation, 1992. ISSN 0027-0644.

DP Dee, SM Uppala, AJ Simmons, Paul Berrisford, P Poli, S Kobayashi, U Andrae, MA Balmaseda, G Balsamo, P Bauer, et al. The era-interim reanalysis: Configuration and performance of the data assimilation system. *Quarterly Journal of the Royal Meteorological Society*, 137(656):553–597, 2011.

Sylvain Delahaies, Ian Roulstone, and Nancy Nichols. A regularization of the carbon cycle data-fusion problem. In *EGU General Assembly Conference Abstracts*, volume 15, page 4087, 2013.

Gérald Desroziers, Loic Berre, Bernard Chapnik, and Paul Poli. Diagnosis of observation, background and analysis-error statistics in observation space. *Quarterly Journal of the Royal Meteorological Society*, 131(613):3385–3396, 2005.

Jean-françois Exbrayat, T Luke Smallman, A Anthony Bloom, and Mathew Williams. Using a data-assimilation system to assess the influence of fire on simulated carbon fluxes and plant traits for the Australian continent. *EGU General Assembly*, 17:6421, 2015.

Andrew Fox, Mathew Williams, Andrew D Richardson, David Cameron, Jeffrey H Gove, Tristan Quaife, Daniel Ricciuto, Markus Reichstein, Enrico Tomelleri, Cathy M Trudinger, et al. The reflex project: comparing different algorithms and implementations for the inversion of a terrestrial ecosystem model against eddy covariance data. *Agricultural and Forest Meteorology*, 149(10):1597–1615, 2009.

Melina A. Freitag, Nancy K. Nichols, and Chris J. Budd. L1-regularisation for ill-posed problems in variational data assimilation. *Pamm*, 10(1):665–668, 2010. ISSN 16177061. doi: 10.1002/pamm.201010324. URL http://doi.wiley.com/10.1002/pamm.201010324.

S.B. Healy and A.A. White. Use of discrete Fourier transforms in the 1D-Var retrieval problem. *Quarterly Journal of the Royal Meteorological Society*, 131(605):63–72, jan 2005. ISSN 00359009. doi: 10.1256/qj.03.193. URL http://doi.wiley.com/10.1256/qj.03.193.

Heikki Järvinen, Erik Andersson, and François Bouttier. Variational assimilation of time sequences of surface observations with serially correlated errors. *Tellus A*, 51(4):469–488, 1999.

Eric Jones, Travis Oliphant, Pearu Peterson, et al. SciPy: Open source scientific tools for Python, 2001. URL http://www.scipy.org/. [Online; accessed 2015-12-04].

Eugenia Kalnay. *Atmospheric modeling, data assimilation, and predictability*. Cambridge university press, 2003.

T. Kaminski, W. Knorr, G. Schürmann, M. Scholze, P. J. Rayner, S. Zaehle, S. Blessing, W. Dorigo, V. Gayler, R. Giering, N. Gobron, J. P. Grant, M. Heimann, a. Hooker-Stroud, S. Houweling, T. Kato, J. Kattge, D. Kelley, S. Kemp, E. N. Koffi, C. Köstler, P. P. Mathieu, B. Pinty, C. H. Reick, C. Rödenbeck, R. Schnur, K. Scipal, C. Sebald, T. Stacke, a. Terwisscha Van Scheltinga, M. Vossbeck, H. Widmann, and T. Ziehn. The BETHY/JSBACH Carbon Cycle Data Assimilation System: Experiences and challenges. *Journal of Geophysical Research: Biogeosciences*, 118(4):1414–1426, 2013. ISSN 21698961. doi: 10.1002/jgrg.20118.

G. Krinner, Nicolas Viovy, Nathalie de Noblet-Ducoudré, Jérôme Ogée, Jan Polcher, Pierre Friedlingstein, Philippe Ciais, Stephen Sitch, and I. Colin Prentice. A dynamic global vegetation model for studies of the coupled atmosphere-biosphere system. *Global Biogeochemical Cycles*, 19(1):1–33, 2005. ISSN 08866236. doi: 10.1029/2003GB002199.

G. Lasslop, M. Reichstein, J. Kattge, and D. Papale. Influences of observation errors in eddy flux data on inverse model parameter estimation. *Biogeosciences Discussions*, 5(1):751–785, February 2008. URL https://hal.archives-ouvertes.fr/hal-00297973.

A. S. Lawless, M.J.P. Cullen, M. A. Freitag, S. Kindermann, and R. Scheichl. *Variational data assimilation for very large environmental problems. In Large Scale Inverse Problems: Computational Methods and Applications in the Earth Sciences.* De Gruyter, 2013.

Yong Li, I. Michael Navon, Weiyu Yang, Xiaolei Zou, J. R. Bates, S. Moorthi, and R. W. Higgins. Four-Dimensional Variational Data Assimilation Experiments with a Multilevel Semi-Lagrangian Semi-Implicit General Circulation Model. *Monthly Weather Review*, 122(5):966–983, may 1994. ISSN 0027-0644. doi: 10.1175/1520-0493(1994)122¡0966:FDVDAE¿2.0.CO;2. URL http://journals.ametsoc.org/doi/abs/10.1175/1520-0493(1994)122%3C0966:FDVDAE%3E2.0.CO%3B2.

LI-COR, Inc. *EddyPro 6 Help and User's Guide.* LI-COR, Inc. Lincoln, NE., 2015.

Andrew C Lorenc and F Rawlins. Why does 4d-var beat 3d-var? *Quarterly Journal of the Royal Meteorological Society*, 131(613):3247–3257, 2005.

P Meir, B Kruijt, M Broadmeadow, E Barbosa, O Kull, F Carswell, A Nobre, and PG Jarvis. Acclimation of photosynthetic capacity to irradiance in tree canopies in relation to leaf nitrogen concentration and leaf mass per unit area. *Plant, Cell & Environment*, 25(3):343–357, 2002.

Alexander J F Moodey, Amos S Lawless, Roland W E Potthast, and Peter Jan van Leeuwen. Nonlinear error dynamics for cycled data assimilation methods. *Inverse Problems*, 29(2):025002, 2013. URL http://stacks.iop.org/0266-5611/29/i=2/a=025002.

I. M. Navon, X. Zou, J. Derber, and J. Sela. Variational Data Assimilation with an Adiabatic Version of the NMC Spectral Model. *Monthly Weather Review*, 120(7):1433–1446, jul 1992. ISSN 0027-0644. doi: 10.1175/1520-0493(1992)120¡1433:VDAWAA¿2.0.CO;2. URL http://journals.ametsoc.org/doi/abs/10.1175/1520-0493(1992)120%3C1433%3AVDAWAA%3E2.0.CO%3B2.

IM Navon. Practical and theoretical aspects of adjoint parameter estimation and identifiability in meteorology and oceanography. *Dynamics of Atmospheres and Oceans*, 27(1):55–79, 1998.

Shuli Niu, Yiqi Luo, Michael C. Dietze, Trevor F. Keenan, Zheng Shi, Jianwei Li, and F. Stuart Chapin Iii. The role of data assimilation in predictive ecology. *Ecosphere*, 5(5):art65, 2014. ISSN 2150-8925. doi: 10.1890/ES13-00273.1. URL http://www.esajournals.org/doi/abs/10.1890/ES13-00273.1.

Jorge Nocedal and Stephen J Wright. *Numerical Optimization.* Springer Science & Business Media, 1999. ISBN 0387987932. URL http://books.google.co.uk/books/about/Numerical_Optimization.html?id=epc5fX0lqRIC&pgis=1.

D. Papale, M. Reichstein, M. Aubinet, E. Canfora, C. Bernhofer, W. Kutsch, B. Longdoz, S. Rambal, R. Valentini, T. Vesala, and D. Yakir. Towards a standardized processing of Net Ecosystem Exchange measured with eddy covariance technique: algorithms and uncertainty estimation. *Biogeosciences*, 3 (4):571–583, 2006. ISSN 1726-4189. doi: 10.5194/bg-3-571-2006.

Tristan Quaife, Philip Lewis, Martin De Kauwe, Mathew Williams, Beverly E. Law, Mathias Disney, and Paul Bowyer. Assimilating canopy reflectance data into an ecosystem model with an Ensemble Kalman Filter. *Remote Sensing of Environment*, 112(4):1347–1364, 2008. ISSN 00344257. doi: 10.1016/j.rse.2007.05.020.

JE Renaud. Automatic differentiation in robust optimization. *AIAA journal*, 35(6):1072–1079, 1997.

Andrew D. Richardson, Miguel D. Mahecha, Eva Falge, Jens Kattge, Antje M. Moffat, Dario Papale, Markus Reichstein, Vanessa J. Stauch, Bobby H. Braswell, Galina Churkina, Bart Kruijt, and David Y. Hollinger. Statistical properties of random {CO2} flux measurement uncertainty inferred from model residuals. *Agricultural and Forest Meteorology*, 148(1):38 – 50, 2008. ISSN 0168-1923. doi: http://dx.doi.org/10.1016/j.agrformet.2007.09.001.

Andrew D Richardson, Mathew Williams, David Y Hollinger, David JP Moore, D Bryan Dail, Eric A Davidson, Neal A Scott, Robert S Evans, Holly Hughes, John T Lee, et al. Estimating parameters of a forest ecosystem c model with measurements of stocks and fluxes as joint constraints. *Oecologia*, 164 (1):25–40, 2010.

Polly J Smith, Sarah L Dance, Michael J Baines, Nancy K Nichols, and Tania R Scott. Variational data assimilation for parameter estimation: application to a simple morphodynamic model. *Ocean Dynamics*, 59(5):697–708, 2009.

Laura M. Stewart, Sarah L. Dance, and Nancy K. Nichols. Data assimilation with correlated observation errors: Experiments with a 1-D shallow water model. *Tellus, Series A: Dynamic Meteorology and Oceanography*, 65(1):1–14, 2013. ISSN 02806495. doi: 10.3402/tellusa.v65i0.19546.

Karl E. Taylor. Summarizing multiple aspects of model performance in a single diagram. *Journal of Geophysical Research*, 106(D7):7183, apr 2001. ISSN 0148-0227. doi: 10.1029/2000JD900719. URL `http://doi.wiley.com/10.1029/2000JD900719`.

Hans Verbeeck, Philippe Peylin, Cédric Bacour, Damien Bonal, Kathy Steppe, and Philippe Ciais. fluxes in Amazon forests: Fusion of eddy covariance data and the ORCHIDEE model. *Journal of Geophysical Research*, 116(G2):1–19, 2011. ISSN 0148-0227. doi: 10.1029/2010JG001544.

J. A. Waller, S. L. Dance, A. S. Lawless, N. K. Nichols, and J. R. Eyre. Representativity error for temperature and humidity using the Met Office high-resolution model. *Quarterly Journal of the Royal Meteorological Society*, 140(681):1189–1197, apr 2014. ISSN 00359009. doi: 10.1002/qj.2207. URL `http://doi.wiley.com/10.1002/qj.2207`.

Sebastian F. Walter and Lutz Lehmann. Algorithmic differentiation in Python with AlgoPy. *Journal of Computational Science*, 4(5):334–344, sep 2013. ISSN 18777503. doi: 10.1016/j.jocs.2011.10.007. URL `http://www.sciencedirect.com/science/article/pii/S1877750311001013`.

PP Weston, W Bell, and JR Eyre. Accounting for correlated error in the assimilation of high-resolution sounder data. *Quarterly Journal of the Royal Meteorological Society*, 140(685):2420–2429, 2014.

M Wilkinson, EL Eaton, MSJ Broadmeadow, and JIL Morison. Inter-annual variation of carbon uptake by a plantation oak woodland in south-eastern england. *Biogeosciences*, 9(12):5373–5389, 2012.

Mathew Williams, Edward B Rastetter, David N Fernandes, Michael L Goulden, Gaius R Shaver, and Loretta C Johnson. Predicting gross primary productivity in terrestrial ecosystems. *Ecological Applications*, 7(3):882–894, 1997.

Mathew Williams, Paul A Schwarz, Beverly E Law, James Irvine, and Meredith R Kurpius. An improved analysis of forest carbon dynamics using data assimilation. *Global Change Biology*, 11(1):89–105, 2005.

J. M. Zobitz, David J P Moore, Tristan Quaife, Bobby H. Braswell, Andrew Bergeson, Jeremy a. Anthony, and Russell K. Monson. Joint data assimilation of satellite reflectance and net ecosystem exchange data constrains ecosystem carbon fluxes at a high-elevation subalpine forest. *Agricultural and Forest Meteorology*, 195-196:73–88, 2014. ISSN 01681923. doi: 10.1016/j.agrformet.2014.04.011. URL `http://dx.doi.org/10.1016/j.agrformet.2014.04.011`.

JM Zobitz, AR Desai, DJP Moore, and MA Chadwick. A primer for data assimilation with ecological models using markov chain monte carlo (mcmc). *Oecologia*, 167(3):599–611, 2011.

Appendix

Parameter	Description	Background	Standard deviation
θ_{min}	Litter mineralisation rate (day^{-1})	$9.810e-04$	$2.030e-03$
f_{auto}	Autotrophic respiration fraction	$5.190e-01$	$1.168e-01$
f_{fol}	Fraction of GPP allocated to foliage	$1.086e-01$	$1.116e-01$
f_{roo}	Fraction of GPP allocated to fine roots	$4.844e-01$	$2.989e-01$
c_{lspan}	Determines annual leaf loss fraction	$1.200e+00$	$1.161e-01$
θ_{woo}	Woody carbon turnover rate (day^{-1})	$1.013e-04$	$1.365e-04$
θ_{roo}	Fine root carbon turnover rate (day^{-1})	$3.225e-03$	$2.930e-03$
θ_{lit}	Litter carbon turnover rate (day^{-1})	$3.442e-03$	$3.117e-03$
θ_{som}	Soil and organic carbon turnover rate (day^{-1})	$1.113e-04$	$1.181e-04$
Θ	Temperature dependance exponent factor	$4.147e-02$	$1.623e-02$
c_{eff}	Canopy efficiency parameter	$7.144e+01$	$2.042e+01$
d_{onset}	Leaf onset day (day)	$1.158e+02$	$6.257e+00$
f_{lab}	Fraction of GPP allocated to labile carbon pool	$3.204e-01$	$1.145e-01$
c_{ronset}	Labile carbon release period (days)	$4.134e+01$	$1.405e+01$
d_{fall}	Leaf fall day (day)	$2.205e+02$	$3.724e+01$
c_{rfall}	Leaf-fall period (days)	$1.168e+02$	$2.259e+01$
c_{lma}	Leaf mass per area (gCm^{-2})	$1.285e+02$	$6.410e+01$
C_{lab}	Labile carbon pool (gCm^{-2})	$1.365e+02$	$6.626e+01$
C_{fol}	Foliar carbon pool (gCm^{-2})	$6.864e+01$	$3.590e+01$
C_{roo}	Fine root carbon pool (gCm^{-2})	$2.838e+02$	$2.193e+02$
C_{woo}	Above and below ground woody carbon pool (gCm^{-2})	$6.506e+03$	$7.143e+03$
C_{lit}	Litter carbon pool (gCm^{-2})	$5.988e+02$	$5.450e+02$
C_{som}	Soil and organic carbon pool (gCm^{-2})	$1.936e+03$	$1.276e+03$

Table 3: Parameter values and standard deviations for background vector used in experiments.